MRI brain image-based segmentation and classification with optimization using metaheuristic deep learning model in Detection of Alzheimer's disease

T Sangeetha Devi[1], V. Raghavendran[2]

[1]Research Scholar, Department of Computer Science, School of Computing Sciences, Vels Institute of Science, Technology and Advanced Studies (VISTAS), Chennai, Tamilnadu 600117,
Email: sangeetha22scholar@gmail.com

[2]Assistant Professor, Department of Computer Science, School of Computing Sciences, Vels Institute of Science, Technology and Advanced Studies (VISTAS), Chennai, Tamilnadu 600117- India,
Email: raghavendran.scs@velsuniv.ac.in

ABSTRACT

A brain condition called Alzheimer's disease results in neuronal malfunctions. Dementia and brain function loss brought on by this illness can worsen memory loss, cognitive decline, and behavioural issues in people. Current techniques for diagnosing Alzheimer's using MRI pictures only use specific, targeted subsets of data depending on factors like gender, age, and other characteristics. They also frequently rely on clinical data to help classify the images. The aim of this research is to propose novel technique in MRI brain image segmentation as well as classification utilizing DL technique with metaheuristic model in optimization for Alzheimer's disease detection. In this proposed model the dataset is collected as well as processed for noise removal and segmentation using fuzzy Gaussian C-adaptive histogram equalization. then the segmented image has been classified using support vector convolutional graph transfer VGG-16 learning and optimized using particle grey wolf firefly optimization. The experimental analysis has been carried out for various brain MRI image dataset in terms of Detection accuracy, mini mental state examination (MMSE), weighted average recognition rate (WARR), recall, AUC. Using T1-weighted brain magnetic resonance imaging, an accurate diagnosis of Alzheimer disease was made possible by an autonomous brain segmentation and classification algorithm based on deep learning. Proposed technique MMSE 90%, Detection accuracy 98%, WARR 95%, Recall 94%, AUC 90%.

Keywords: MRI brain, image segmentation, classification, deep learning technique, metaheuristic model, Alzheimer's disease detection

1. INTRODUCTION

Mild cognitive impairment (MCI) is thought to be a transitional state between normal cognition as well as early stages of dementia. Alzheimer disease (AD) is most frequent cause of dementia. Even though the available treatments and preventive measures are only marginally successful, a trustworthy diagnostic method for making decisions is crucial in the early stages of AD. In neuroradiology, magnetic resonance imaging (MRI) is frequently utilised to identify brain abnormalities such as stroke, vascular disease, tumour tissue. Nevertheless, MRI has proven less effective in definitively diagnosing degenerative illnesses, such as Alzheimer's disease (AD), mostly due to the disease's diffuse fingerprints in MRI images that make it difficult to differentiate between disease and normal ageing [1]. Small datasets have been utilized to train ML as well as DL techniques, but this lack of training data frequently results in poor generalisation performance on new datasets that were not utilized to train methods. According to guidelines of Alzheimer's Association and National Institute on Ageing, MR imaging can be a useful imaging modality in the diagnosis process for patients diagnosed with AD and MCI. When it comes to AD diagnosis, imaging biomarkers are crucial in both clinical and research settings. Understanding pathophysiologic mechanisms behind AD as well as its early diagnosis, particularly in preclinical or prodromal stage, has greatly advanced with the discovery of amyloid and the t PET ligand [2]. While t and amyloid PET offer greater sensitivity and specificity in AD diagnosis, their application in clinical practice is restricted due to their high cost, scarcity, and need for ionising radiation. Significant biomarkers that might be utilised for AD diagnosis in a clinical research environment include CSF t and amyloid. CSF AD biomarkers are likewise not widely available, yet. On the other hand, MR imaging is

often accessible and employed in routine practice to bolster the diagnosis of AD and rule out alternative explanations of cognitive impairment, such as vascular dementia, stroke, normal-pressure hydrocephalus, inflammatory, and neoplastic disorders [3]. It is vitally crucial to accurately diagnose AD in its early stages utilising a widely accessible, non-invasive method. Given that structural MRI is more widely available and non-invasive than PET, it is a more viable option for imagingbased supplementary diagnosis for AD. Additionally, it is possible to include MRI markers into autonomous end-to-end DL methods thanks to well-developed pipelines for preparing MRI data. Automated voice recognition, aftershock pattern prediction, severe weather condition prediction are just a few of the real-world applications where deep learning has already proven effective [4]. Convolutional neural networks (CNNs) are a popular design that works well for image-based deep learning. In clinical settings, CNNs have been used to objectively diagnose retinal illnesses, screen for breast cancer, and diagnose skin cancer.

Nevertheless, previous attempts to diagnose AD using MRI have not yet proven to be clinically useful. The inability of brain MRI-based algorithms to generalise is a significant problem, particularly if they were trained on sparse data. For instance, a classifier based on brain imaging might provide accurate forecasts for testing samples obtained from a particular hospital where training dataset was obtained. When classifier is directly applied to samples from an unidentified hospital, its performance drastically decreases [5]. A major contributing factor to performance discrepancies is the fact that brain imaging data vary depending on scanner variables, such as vendor, fled of view, voxel size, applied gradient fields, hardware of the head coil, pulse sequence, and scanning parameters. The participants' sex, age, race/ethnicity, and educational background also vary. Sturdy techniques must function well on a variety of populations. A brain imaging-based classifier trained on data from one site finds it challenging to generalise to data from unseen sites/scanners due to these variances in the scans and in the populations investigated. This has hindered the practical utility of brain imaging-based classifiers in clinical contexts [6].

Major contribution of this research is as follows:

In this research, a model is proposed to determine as an output whether an individual has mild, moderate, or no AD based on brain MRI sample pictures. To provide a novel method for segmentation and classification of MRI brain images that combines a metaheuristic optimisation model with deep learning techniques. This model suggests utilising fuzzy Gaussian C-adaptive histogram equalization to collect and process the dataset for segmentation and noise removal. Particle Grey Wolf Firefly Optimisation was used to optimize the segmented image after it had been classified using support vector convolutional graph transfer VGG-16 learning.

2. RELATED WORKS

Deep Learning (DL) techniques are among the latest advancements in ML that have been introduced. To prevent bottlenecks during diagnostic support, work [7] suggested using autoencoders with Softmax output layers in their medical applications. Convolutional networks are widely used because they are the most suited kind for processing pictures and signals, as demonstrated by the research done by [8] and others. Author [9] suggested that to enhance performance of a traditional ML classifier, limited Boltzmann machines should be used as an initial step. The study examines the effectiveness of health recommendation systems that utilise deep learning-based collaborative filtering approaches. The task involves comparing several models to identify the most efficient method for providing personalised health recommendations. The study assesses parameters including as accuracy, precision, recall, and F1-score. The results demonstrate that deep learning models surpass standard collaborative filtering methods, providing improved accuracy and more pertinent health recommendations. The results emphasise the capacity of deep learning to greatly enhance user experience in health recommendation systems by offering more personalised and precise guidance derived from individual health data and inclinations [10, 11, 12]. Other approaches, like the one from [13], were able to acquire information from a vast portion of brain despite computing cost by using grey matter volumes rather than MRI images for diagnosis of AD. Information from a variety of medical imaging modalities, such as integrated data from horizontal MRI images as well as their matching positron-emission tomography (PET) images, was recovered in this work and in several other proposals. In addition to being used to diagnose AD, DL has also been used in conjunction with MRI images for other neuroscience-related purposes, as demonstrated in [14], where a technique for identifying activity variations in different brain regions during rest was suggested. The features in [15] were extracted using a three-dimensional discrete wavelet transformation (3D DWT). A 1D DWT was applied to each dimension in order to achieve this. Subsequently, volumetric feature extraction was carried out by first obtaining energy, variance, Shannon entropy of each brain image's 80 sub-band. The triplet was then fed into a principal component analysis

(PCA) module to reduce its dimensionality. After that, an SVM was employed to complete the classification. The study [16] employed a Support Vector Machine (SVM) for classification as well as independent component analysis (ICA) for feature attraction and picture decomposition. They used the shape of a brain to build a tree, and the feature vectors were the branches that corresponded to the desired classification. In [17], an entirely different approach was taken, utilising a Genetic Algorithm (GA) to investigate possible feature combinations and then voxel selection and Voxel-Based Morphometry (VBM) for extraction. The Extreme Learning Machine (ELM) was assembled by this group [18]. According to work

[19], sequential learning is a more effective method. It used a radial basis function network (PBL-McRBFN) in conjunction with a projection-based metacognitive learning method. Because of their procedure, the training samples could be utilised only once while they were available and then thrown away right away. In [20], features were extracted using voxelbased morphometry as well as deformation-based morphometry. The classification was then accomplished using a lattice computing method that included a meta representation with interval numbers, extraction, dimensionality reduction, k closest neighbours (k-NN). Because they erroneously assume feature independence, classifiers based on the Naive Bayes theorem belong to the standard family of probabilistic classifiers. It has been demonstrated that the researchers' Bayesian network decision model [21] works better than other well-known classifiers. Despite the fact that [22] presented a multifold Bayesian Kernalization technique that can more accurately distinguish AD from NC, they discovered inadequate outcomes in the identification of MCI-converter. Principal component analysis (PCA) was utilised in Work [23] to minimise the feature space after digital wavelet transform was performed to extract features. The author [24] suggested applying deformation-based morphometry (DBM) approaches and suggested five features: the displacement field's magnitude, the Jacobian map, modulated GM (MGM), trace of the Jacobian matrix (TJM), and geodesic anisotropy (GEODAN). They also recommended using WTT, Bhattacharyya distance (BD), and

Pearson's correlation (PEC) to gauge importance of voxel sites. A method to identify Alzheimer's illness was claimed by Work [25]. He used a five-stage machine learning pipeline technique for the detection, with a sub-stage for each step. This pipeline was subjected to several classifier applications. His conclusion was that the performance measures of the random forest classifier were superior. Author [26] compared the performance of imputation and non-imputation approaches using the Random-Forest classifier. They found that 87% accuracy is obtained by the imputation approach and 83% accuracy is obtained by the non-imputation method. Additionally, it categorised the subjects as either non-demented or demented. A multi-atlas method for detecting Alzheimer's disease was proposed in Work [27]. It employed PCA and cast-off SVM for classification to classify the distinct features extracted from each atlas template as well as combined characteristics of 2 atlases. They were 94% accurate in the AD vs. CN test, 76.5% accurate in the CN vs. MCI test, 75.5% accurate in MCI vs. AD test. They noticed that compared to the single-atlas strategy, the multi-atlas approach produced better outcomes. In his study, author [28] claimed that early detection can stop spread of illness. He used structural MRI to pull brain scans from repository. He proposed projecting data onto the available linear space using kernels. After that, he used a Support Vector Machine (SVM) to categorise the information. For his categorisation, he achieved a good accuracy of 93.85% with high sensitivity and specificity. Their suggested strategy aims to promptly identify these cardiac anomalies in order to prevent potentially lethal outcomes. The subsequent stage involves assessing whether or not the user is susceptible to acquiring cardiovascular disease [29].

3.   Background on AD detection using brain MRI image segmentation and classification

AD detection system, a complex and all-encompassing structure intended to enable the effective identification of AD, is depicted in Figure 1. This system leverages the synergistic integration of critical elements, such as deep learning models, assessment, data management strategies, preprocessing techniques, and brain scans. When combined, these components give the system a strong base that guarantees its efficiency, dependability, and accuracy.
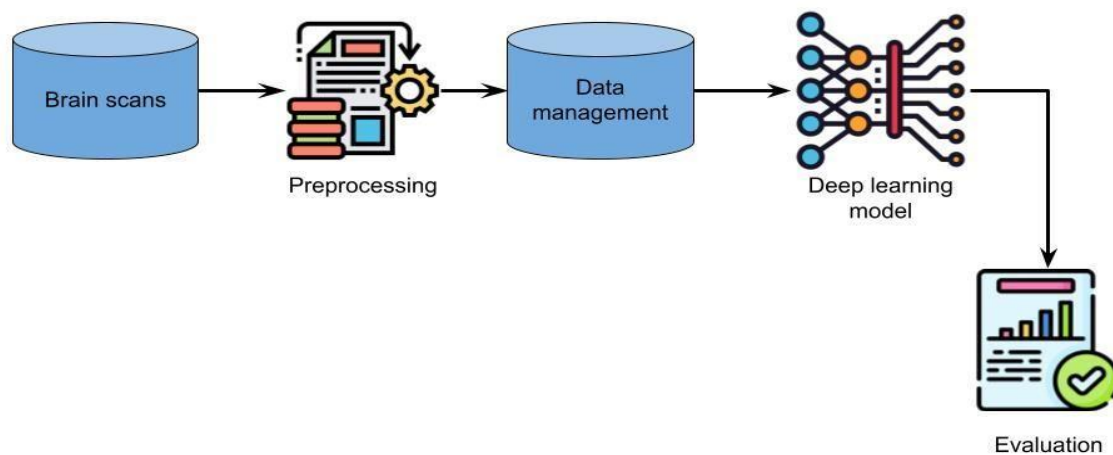
Figure 1. The Architecture of AD detection system

Because deep learning approaches may produce strong results over a large amount of data, they have attracted interest in classification of AD and in segmentation of brain's structure. Thus, DL techniques are currently preferred over state-of-the-art ML techniques. Our aim is to provide an overview of the most recent deep learning-based brain MRI segmentation methods for the quantitative assessment of brain MRI in relation to AD diagnosis. An integrated approach promotes early identification and individualized treatment plans while working to increase the precision and dependability of AD categorization. This study aims to assess how well the suggested method performs in AD categorization as well as investigates how it might improve AD diagnosis. By comparing the outcomes with other cutting-edge segmentation techniques, parameters including accuracy, sensitivity, and specificity are assessed. Through the use of cutting-edge computational approaches, this research seeks to improve illness diagnostics and progress the diagnosis of AD. First, we train entire network on training set, then we use validation set to fine-tune it during model training and optimisation phase. Appropriate optimisation procedures, such as stochastic gradient descent, in conjunction with well chosen learning rates, batch sizes, training iterations, are utilized to improve method performance and generalization. To further improve the model's overall performance, more optimisation techniques like learning rate decay, weight decay, and early halting are used.

4.   Proposed MRI image analysis in Alzheimer's disease detection

Procedure of acquiring data to compile dataset needed for diagnosis is the initial step, as seen in Fig. 2. Preprocessing the dataset is the second step, which aims to improve its quality and the classification task's performance. The dividing stage is the third phase. Subsets of the dataset for testing, validation, and training can be separated. The final step is a learning system that uses appropriate and targeted methods to divide up the features, extract knowledge from the data, adjust the settings, and categorise the illness into a certain class.
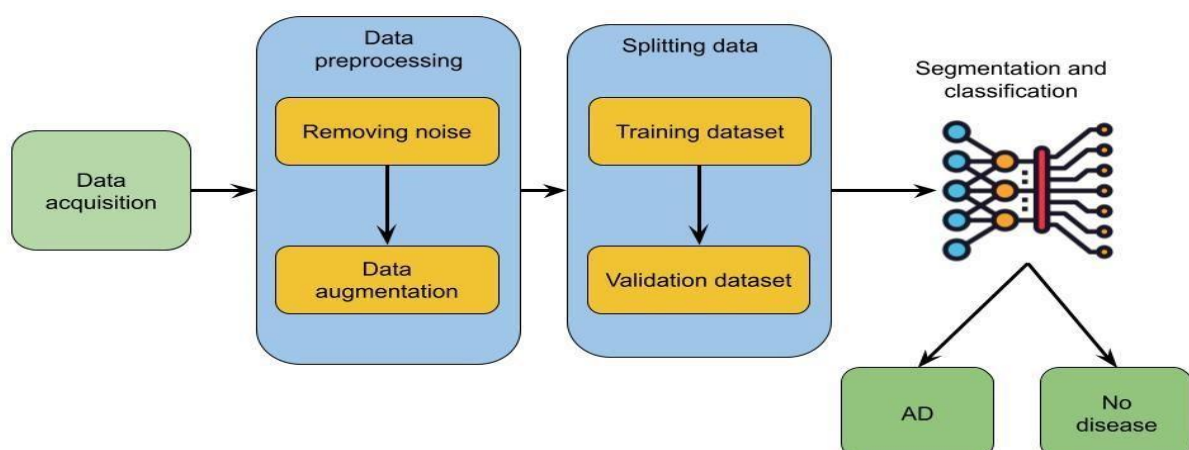
Figure 2. Proposed MRI image analysis in AD detection

The pre-processing steps required to improve MRI data standardisation are as follows: first, all MRI data were spatially normalised using Statistical Parametric Mapping12 (SPM12), ensuring that every image voxel matched with same anatomical position. Subsequently, extension of SPM12, the Computational Anatomy Toolbox12 (CAT12), was used to exclude the skull and cervical regions from the image. CAT12 employed the voxel-based morphometric (VBM) technique to generate a grey matter template. Furthermore, the MRI pictures were divided into three segments: CSF, WM, and GM (grey matter). For the GM ICBM-152 standard template, GM pictures were chosen as well as registered using the nonlinear affine transition. Each 3D GM was averaged, scaled, and concatenated into a stack of 96 × 96 × 96 voxels with voxel-sizes of 1.5 mm (axial), 1.5 mm (coronal), and 1.5 mm (sagittal). Stack was smoothed using the Gaussian kernel, yielding a full width at half maximum (FWHM) of roughly 7 mm. Our study trained using 62 × 96 × 96 slices from the middle of the stack, which contain the thalamus, hippocampus, and other key brain tissue related to memory.

Pre-processing: Each pre-processed T1-weighted volume had a voxel size of 1mm × 1mm × 1mm and a data matrix size of 176 × 208 × 176. We chose the 106th, or middle axial slice, from these volumes to use as the input for our models. It has been demonstrated that this axial location correlates to the anatomical slice, which, because of its high individual content-based picture retrieval performance, has a larger degree of disease linked information. The mean average precision values for the axial plane are used to evaluate the performance results when the disease label was utilised as the criterion of interest. This result was taken to mean that they had a greater level of disease-related knowledge, which qualified them for a single-slice categorisation approach. It should be mentioned, nevertheless, that the dataset or atlas that is utilised has a significant impact on how many slices are chosen. The process we used to choose our single slice contender was the same. The MRI slices in the dataset are normalised in the interval [0,1] before being fed into the network, providing an unvaried contrast and intensity range.

5. Fuzzy Gaussian C-adaptive histogram equalization (FGCAHE) based segmentation

The goal of cluster reduction in FCM is to merge smaller colonies into larger colonies by utilising their shared characteristics. Because K-Means has assisted in part of the FCM clustering process, this strategy reduces the weight of search process on FCM as well as reduces number of repetitions. The way FCM groups data is by calculating weight from every individual data point to centroid. Objective function of C-means, such as one in formula (1), is minimised to produce fuzzy C-means.

$$J_m = \sum_{i=1}^{N} \sum_{i=1}^{c} u_{ij}^m \|x_i - c_j\|^2 \qquad (1)$$

Uij denotes degree of membership of each data point, and for each x, which is a collection of data points, c is cluster centre point and m is a greater real value of $\sum x\_i-c\_i \sum{}^2$, which is distance between data points as well as cluster centre point determined by Euclidean formula.

The FCM membership function can be expressed as eqn (2).

$$u_{ij} = \frac{1}{\sum_{k=1}^{c} \left(\frac{\|x_i - c_j\|}{\|x_i - c_k\|}\right)^{\frac{2}{m-1}}} \qquad (2)$$

One significant drawback is that it lacks spatial context information, making it vulnerable to noise and image artefacts. Each class in FCM is assigned a set of pixels using fuzzy membership functions. For example, X = {x1, x2..., xN} represents a picture of N pixels that needs to be split up into c clusters. It is customary to pass number of clusters as an input parameter. The process of fuzzy partitioning a given data set involves minimising objective function for a predetermined number of clusters, while adhering to restriction that total membership grades of data within a cluster must equal 1. where n is number of data points; m is fuzzier value; c is number of cluster centroids or data subsets; V is matrix of cluster centroids, while U is fuzzy partition matrix. Fuzzy membership value of pixel k in cluster i is denoted by Uik. Following restrictions are satisfied by this membership value by eqn (3)

$0 \leq U_a \leq 1$. for $1 \leq i \leq c$, $1 \leq k \leq n$.

$0 < \sum_{i=1}^{n} U_d < n$, for $1 \leq i \leq c$

$\sum_{i=1}^{n} U_{it} = 1$, for $1 \leq k \leq n$.

$v_i = \sum_{i=1}^{n} (w_N)' x_1 / \sum_{i=1}^{n} (\omega_i)'$

$$\omega_{ik} = \left(\sum_{i=1}^{c} \left(\frac{d4}{d_{jk}}\right)^{-2(U-1}\right)^{-1} \tag{3}$$

The following is the criteria for termination. The formula is U (t+1) ik – U (t) ik< ε, where ε is a small value that can be specified during initialisation and is the Euclidean norm. A weighted sum of c Gaussian density distributions makes up GMM. The probability of observed data I(k) using the GMM is as follows:

$P(I(k) \mid \Theta_i) = \sum_{i=1}^{c} p_i N(I(k) \mid \mu_i, \Sigma_i)$

GMM's parameters, represented by Θ = {Θi,i = 1,...,c}, are often evaluated by using EM algorithm to maximise likelihood of observed data, as demonstrated below eqn (4)

$\Theta^* = \arg\max \prod_{i=1}^{n} \left[\sum_{i=1}^{c} p_i N(I(k) \mid \mu_i, \Sigma_i)\right]$ (4)

Let pi(x) represent the prior probability p (y ∈Ωi ∩ Ox). p(I(y)|y ∈Ωi ∩ Ox) has a Gaussian distribution N(I(y)|μi(x), Σi(x)) with mean μi(x) and covariance matrix Σi(x), according to the GMM assumption. By minimising the following energy function and applying natural logarithm to both sides of the equation, we may determine maximum a posteriori probability (MAP) solution to this segmentation issue by eqn (5)

$E_x^{\text{LGMM}} = \sum_{i=1}^{c} \int_{Q, 0,} -\ln[\, p_i(x)N(I(y) \mid \mu_i(x), \Sigma_i(x))]dy$ (5)

When c i= pi(x)=1 is satisfied and pi(x) is the mixing coefficient. In order to apply bias field correction to the segmentation procedure, we consider each tissue type I's true intensity J to be a constant vi. So, the following approximations can be used to determine mean of observed data in every Gaussian component by eqn (6)

$\mu_i(x) = b(x)v_i, i = 1, \dots, c$ (6)

where bias field at each voxel x is denoted by b(x). The histogram is flattened using the HE method in accordance with the contrast and intensity level range of the image. Number of pixels ni with intensity level i, as described by Eq. (7), yields picture histogram H(i) for intensity level i, where L is maximum range of grey level.

$H(i) = n_i, \text{ for } i = 0,1,2, \dots, (L-1)$ (7)

Histogram is divided based on number of pixels with a specific intensity, using Eq. (7). Equation (7) utilises these findings to determine probability px(i) of pixel i, which is subsequently utilised to compute cumulative distribution function (PDF) in Equation (8). As distribution of equalisation histogram (Eq. (8)), CDF has a value in range of 0–255.

$p_x(i) = p(x = i) = n_i/n$

$cdf_x(i) = \sum_{j=0}^{i} p_x(x = j)$

$h(v) = \text{round}\left(\frac{cdf(v) - cdf_{\min}}{n - cdf\min}\right)$ (8)

AHE modifies the histogram by utilising a lower threshold value. By minimising edge shadowing and avoiding over-enhancement of noise, AHE enhances contrast-based image outcomes. The clip limit from Eq. (9) is used to get the limit value.

$\beta = \frac{M}{n}(1 + \frac{\alpha}{100}(s_{\max} - 1))$ ~~(9)~~

where n is 8-bit greyscale value (0–255) and M is the region's area. With a range of 0–100, α is upper limit of clip factor that is utilised as a boundary on histogram.

6. Support vector convolutional graph transfer VGG-16 learning (SVCGTVgg-16) model in classification

Normalisation of regional volume by intracranial volume is essential in neurodegenerative research to minimise interindividual variation. We created a brain-extraction technique, which is another DL-based semantic segmentation method, to quantify whole-brain volumes. The raw brain parcellation volumes were divided by the total brain volume. Additionally, we combined 82 volumes, age, sex (0 or 1) as input variables for classification in order to exclude age-related impacts on brain volumes as well as reflect sex matching. It uses a multivariate method of matching sex and age. The dimensionality of the data is decreased by transforming every T1-weighted brain MR image into volume of every brain region. Boosting strategy is effective for classifiers when the dimensionality of the data is relatively minimal.

SVMs can be used for both straightforward, linear classification tasks and more difficult, or nonlinear, classification problems. In the linear as well as nonlinear cases, SVMs handle both separable and non-separable issues. Mapping is accomplished by choosing an appropriate kernel function. T = x1, y1, • • •, xn, yn is a linearly separable sample set, where xi, yi denote the sample point, xi ∈ R n, and yi∈ {+1, −1}, i = 1, 2, • • •, n. Two different kinds of training samples are shown by red and black circles, respectively. Currently, there are an endless number of interfaces available that can accurately distinguish between the two kinds of samples. Therefore, the best possible classification hyperplane is needed, one that

minimises actual risk while meeting the maximum classification interval and guarantees the least amount of empirical risk while accurately dividing the two categories of samples. The optimal hyperplane, at which the solution is unique, is found using the maximum classification interval in the fundamental principle of linear separable SVM.

The final GCN layers were gradually adjusted while the initial few layers were left unchanged, using a layer-by-layer fine-tuning technique. Transfusion (10), a different kind of transfer learning that only transfers the initial few GCN layers while training the remainder of the network using random initialisation, was also examined. The delegate component of whole convolutional neural network is the CONV layer. To this layer, an image (224 224 3) is supplied. This layer's primary goal is to extract identification local information from the input channels or grids that are received. It is expected that each kernel will carry out a convolution operation in order to extract local features. The dot product between weights of neurones and a tiny region in input volume to which they are attached is computed. In the first convolutional layer of the designed model, there are 64 kernels overall. In the second, third, fourth, and fifth layers, there are 256 kernels total. In the sixth and seventh layers, there are 4096 kernels altogether. In addition to multiple kernels, the kernel size in first layer is (11⬜ 11) pixels; in second layer, this is decreased to (5⬜ 5) pixels, and in the remaining layers of CNN, it is further reduced to (3⬜ 3) pixels. Kernel size of the last convolutional layer is (6⬜6) pixels.

A feature extraction layer, a batch normalisation layer, an activation layer for rectified linear units (ReLUs), and a dropout layer are present in every convolutional block. Every convolutional block, other from third and fourth convolutional layers, is succeeded by a maxpooling or down-sampling layer. Convolution operations are carried out on the images by convolutional or feature extraction layers. They involve pixel-wise multiplications, the extraction of the most significant features using a specific number of kernel filters, striding, padding. Convolution has the following definition by eqn (10)

$$B(i, j) = \sum_m \sum_n K(m, n) \cdot A(i - m, j - n) \qquad (10)$$

Before images are down-sampled, these layers' various kernel filters can identify as well as extract key characteristics from original images. Effective back-propagation is supported by the activation function provided by the ReLU activation layer, which allows weights to be updated without vanishing gradient problems during training. By discarding some weights along with their corresponding neurones, dropout layer helps keep the network from overfitting. The meaning of the ReLU activation function is as follows: $Y_i = \max(x, 0)$ and $x = w_i x_i + b_f$ where w is weight of network in size, x is input image, b is bias term and Y is ReLU activation function. After taking a sample of the convolutional block's output features, the max-pooling layer applies a pooling filter with a predetermined number of stridings. By choosing highest pixel values for optimisation, this minimises the features. A maximum pooling example with a stride size of [2x2] and a pooling size of [4x4]. By applying a pooling filter to convolved feature from convolutional layer as well as highest pixel value, it uses a location-invariant down-sampling technique. Here is how downsampling is defined by eqn (11) $I(x, y) = \left[\dfrac{A_x \cdots - P}{s} \right]$ (11)

Definition of a graph G: G= (V, E) is a set of nodes, or vertices, denoted by V and edges, represented by E. Both directed and undirected edges are possible. A very flexible data structure is a graph. Different real-life entities, like social media networks, chemicals, even photographs, can be represented by it. In our work, we represent the image dataset using a graph data structure, and then we perform various operations on it. GNN is a member of a class of DL methods that may perform node-level or edge-level prediction tasks when directly applied to graph data. Graph data differs greatly from the traditional data that we often feed into NN for the following main reasons: 1. The size of graph data is not finite. The number of nodes in a graph dataset might vary in its dimension. However, we need a neural network that can handle any number of input dimensions. 2. Isomersofracial graphs Because the graph data structure is isomorphic, the image can actually change depending on which order the graph is traversed. Therefore, the graph representation cannot be satisfied with a single adjacency matrix.

Graphs are inherently non-Euclidean. This indicates that there is no fixed distance between any of distances in graph and that they are non-Euclidean in nature. The aforementioned factors make it challenging to apply traditional ML as well as DL methods to graph data structures. GNNs are a component of representation learning, which effectively addresses every one of the problems that the graph data structure in deep learning faces. Nodes in a graph neural network can talk to one another and exchange information about themselves.

The graph is based on idea of node embeddings, whereby nodes are mapped to a lowdimensional, d-dimensional embedding space rather than the actual dimension of the graph in question. Because of this, comparable nodes are implanted near to one another. In this manner, a graph NN is utilized to solve pixel similarity issue. Think of nodes a and b in our graph. Two feature vectors, Xa and Xb, are associated with

these nodes. Following the passage of these feature vectors through encoders, the original features are transformed into embeddings, which are then categorised according to how similar the features are.

An approach that is frequently used to deal with small amounts of training datasets is transfer learning. In reality, CNN models can be trained using fine-tuning method using pretrained methods or from scratch using random parameter initialisation. We know from domain expertise of medical research that both sMRI and MD may detect the shrinkage of hippocampus region of interest (ROI) that coincides with the onset of AD. It shows two participants as examples: an AD subject on the right and a normal control (NC) subject on the left, using both modalities (sMRI scan in (B) and an MD map in (A). It displays the hippocampus region from various angles of projection. Additionally, Axial, Sagittal, Coronal planes, in that order, from top to bottom. As the example image shows, the hippocampal atrophy can be distinguished between the two modalities by maintaining same form but reversed representation. This indicates that signal generated by CSF flows around hippocampal region is seen as a bright region on MD maps but as a dark region on sMRI scans.
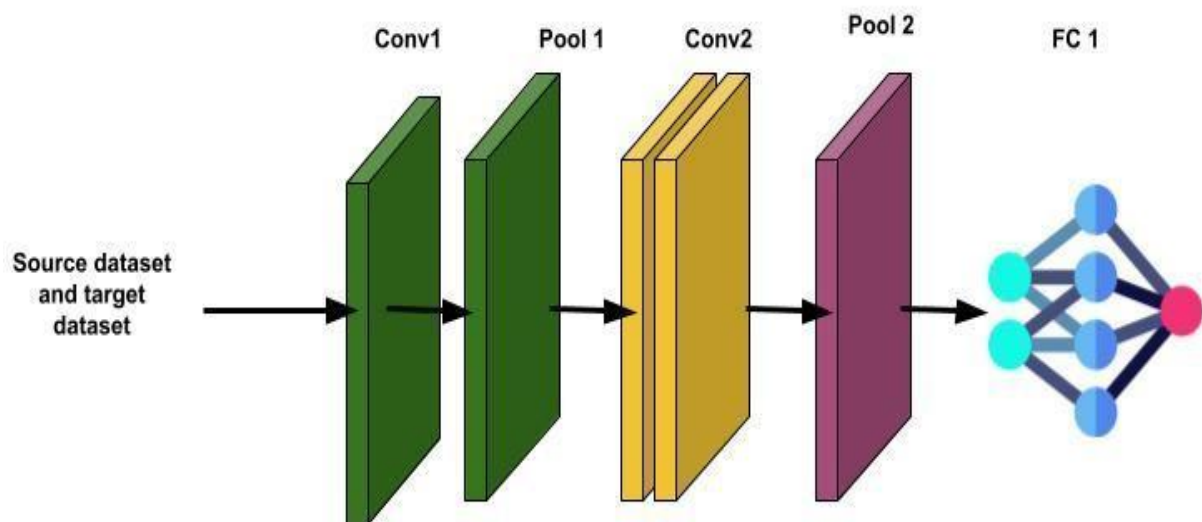
Figure 3. scheme of Transfer Learning for parameters optimization

This phenomenon is demonstrated in Figure 3, which shows two subjects: an AD subject on the right and a normal control (NC) subject on the left, both using the same modalities—an sMRI scan (B) and an MD map (A). Because of this, we may start with learnt methods in source domain of sMRI and move them towards the goal domain of MD using a method called cross-modal transfer learning to transfer learning between these two types of data by eqn (12)

$$\{^{W0-W\phi'} \qquad (12) \quad Wi+1-F(Wi)$$

We start training with parameters of $W'\phi$, where $W'\phi$ is best trained method on big sMRI dataset, fine-tune all or partial layers of employed architecture. F is method for optimisation. The following is the definition of the weights update formula by eqn (13)

$$V_{i+1} + \mu V_i - \alpha\nabla J(W_i + \mu V_i)$$
$$W_{i+1} - W_i + V_{i+1} \qquad\qquad (13)$$

where v is velocity, y is momentum, c is learning rate, and d is the set of parameters for each layer at iteration d. Figure 4 shows how specifications in our CNN architecture are transferred. The optimisation process for every convolutional as well as fully connected layer is shown by the arrows.
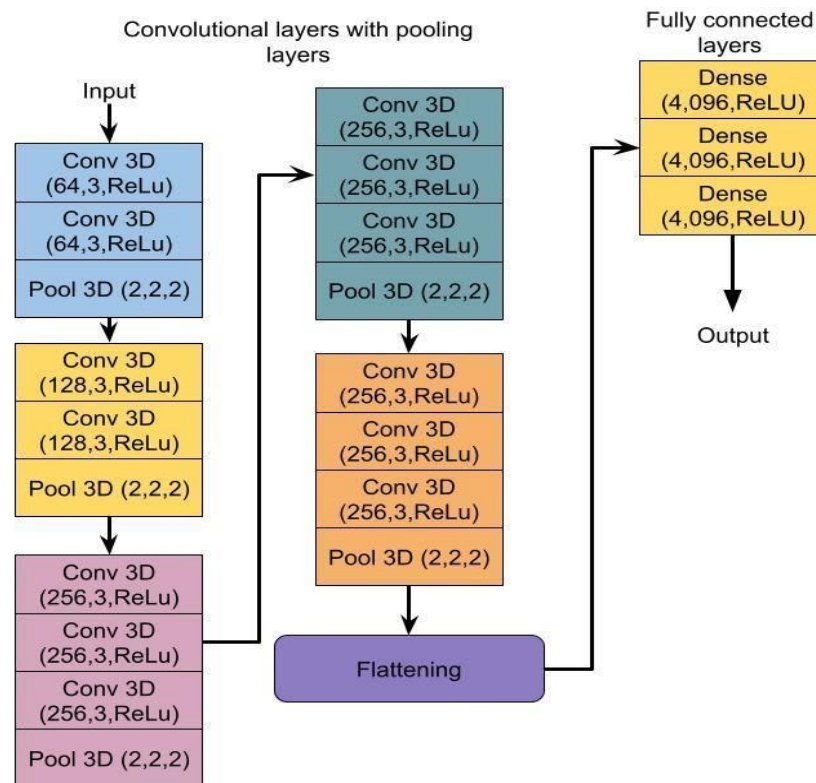
Figure 4. Architecture of VGG-16

(A) An RGB image of a defined size serves as input for first Conv3D. Image is passed through a stack of convolutional layers, where number of filters and filter size are indicated. The spatial 3D pooling layer comes after the convolution layers. Pooling is done with stride 2 throughout the 2 × 2 × 2-pixel window. The image's boundaries and shape are maintained by this layer; 2D feature maps are flattened into a 1D feature vector by flattening layer (B), and then they are sent to fully-connected layers (C). Every hidden layer has a ReLU function, which makes it possible to solve the vanishing gradient descent issue and improve learning. Nonlinear softmax function, which provides probability distribution of classes, is present in last layer. Anticipated class will be determined by looking at the class with the highest likelihood. Conv: layer of convolution

VGG-16: A feature extractor based on pretrained VGG-16 method was employed in this investigation. Additionally, a bootstrap feature extractor with pretrained weights, VGG-16, was employed to extract features from the pre-processed brain sMRI images. VGG-16: In this study, a feature extractor built on top of pretrained VGG-16 method was used. Furthermore, features were extracted from pre-processed brain sMRI images using the bootstrap feature extractor with pretrained weights, VGG-16. After that, a fresh classifier that had been trained from scratch was given the retrieved features. It's crucial to remember that VGG-16 method is a pretrained method with a set input configuration, so the greyscale picture dataset could not be fed to it directly. RGB photos with three channels are needed as input for VGG-16. In contrast, a greyscale image contains a single channel. Repetition of all picture arrays in dataset three times repeatedly on a new dimension is obvious approach. Consequently, the identical image would show up across all three channels. To achieve this, the colour mode was set to "RGB" in the flow from directory method of the Keras library.

7. Particle Grey Wolf Firefly Optimisation (PGWFO) model

PSO is a population-based algorithm that outperforms a general method in terms of convergence speed. It draws inspiration from flocks of birds and schools of fish. The initial placement of particles is random, and they are updated iteratively in terms of both position and velocity. The terms "pbest" and "gbest" denote the locations of the updated and current particle systems, respectively. By incorporating a "stop" condition based on a bisection approach, PSO lowers the number of iterations necessary. The procedure is then stopped after approximating the chosen values; each iteration's accuracy is roughly equal to the preceding one. The ith particle's revised position is calculated as follows by eqn (14)

$$V_{ij}(s+1) = x \cdot V_{ij}(s) + a1 \cdot R1.(I_{im}(s) - y_{im}(s)) + a2 \cdot R2.(g_{im}(s) - y_{im}(s))$$

$$y_{im}(s+1) = y_{im}(s) + V_{ij}(s+1)$$

$x\max - x\min$

$$x(s) = x_{\max} = \underline{\hspace{3cm}} T, s \qquad (14)$$

Maximum iteration time (T), higher limit (xmax), lower limit (xmin) are indicated below. Each solution during feature selection is a subset of features. Every set of particles has a certain position, and each set is represented as a binary vector. The Mth position rejects the Mth characteristic. The PSO selects features by starting with a random solution and working its way up to the optimal global solution, which is represented by a fresh subset of features. Every feature has a link to a dataset that takes up space in the search. The Mth position determines whether a feature is deemed informative or not; if it is 0, the feature is not deemed informative. The Mth feature is not appended to the s if the Mthposition is −1. A well-known meta-heuristic algorithm, the GWO simulates the hunting and leadership styles of grey wolves. There are four levels in GWO: the alpha (α) level is the first, where the troop leaders (male or female) are identified as the α wolves. They also possess the ability to make decisions about where to hunt, how long to walk, where to sleep, and other matters. Known as beta (β), the second level assists α in making decisions. Third level, also referred to as subordinates, is called delta (δ). Omega (ω) is the final level and is referred to as scapegoat. All three of these parameters—α, β, and δ—serve as hunting method guides in the GWO algorithm. Equation (15) displays the mathematical description of encircling behaviour.

$$\vec{A} = |\vec{B} \cdot \hat{X}^r(tr) - \bar{X}(tr)$$

$$\vec{X}(tr+1) = \vec{X}'(tr) - \vec{C} \cdot \vec{A} \qquad (15)$$

where tr stands for the current iteration, C and -B for coefficient vectors, P X for the prey's position vector, X for grey wolf's position vector. The evaluation of C and B is specified in Eqs. (16), where 1 v and - 2 v are random vectors in range [0, [1]], and mi is linearly minimised from 2 to 0.

$$\bar{C} = 2mi \cdot \vec{v}_1 - mi$$

$$\vec{B} = 2 \cdot \vec{v}_2 \qquad (16)$$

In general, the hunting process is guided by α. The top three solutions are retained from the search space, and the corresponding update strategy is evaluated using the formulas found in Equations (28–30).

8. RESULTS AND DISCUSSION

Hardware configuration: The studies were carried out using a GPU-based high-performance computing platform with two Nvidia TESLA P-100 graphics cards with 16 GB dedicated memory, an Intel(R) Xeon(R) CPU E5-2680 v2 @2.80GHz processor, and 187 Gb of RAM. With a batch size of 64 samples, the average computing time for one epoch during training phase is 2.03 seconds. For MRI pretreatment and CNN algorithms, Think Server TS560 running Linux (Ubuntu 16.10) was utilised. This system had a high-performance GPU, NVIDIA Tesla P40, with 3840 CUDA cores, high-frequency Intel Xeon E5-2650 V4 processor with 128 GB of total memory. Python 2.7.12 was used to implement all of the techniques. Using TensorFlow-based deep learning, NN is constructed using Keras package. When analysing imaging data, analysts were blinded to identities of all subjects.

Dataset description: Segmenting and categorising brain tissue types as well as classifying patients with AD are done using the data assessment framework of three-dimension (3D) cross-sectional brain MRI. Brain MRI segmentation and AD diagnosis are commonly achieved through publicly available datasets like the internet brain segmentation repository (IBSR), medical image computing and computer-assisted intervention (MICCAI),

Alzheimer's disease neuroimaging initiative (ADNI), open access series of imaging studies (OASIS). Information for OASIS, ADNI, IBSR, MICCAI datasets is displayed in Table 1. Below is a description of these datasets, which is followed by a step-by-step examination of brain MRI results.

Table 1. Details of OASIS, ADNI, IBSR, and MICCAI datasets

Dataset	Class	Subjects	Sex		Age		MMSE		MRI scans
			M	F	Mean	std	Mean	std	
OASIS	AD	102	42	61	56.56	5.09	22.25	5.17	103
	HC	315	112	198	46.26	21.12	27.63	1.93	315
ADNI	AD	190	114	93	72.1	8.6	21.4	2.5	535
	MCI	395	267	143	75.6	5.6	30.5	2.2	1012
	HC	225	110	111	77.9	5.2	31.2	1.5	879
IBSR	HC	15	16	7	75	-	-	-	16
MICCAI	HC	32	-	-	-	-	-	-	39

OASIS

AD Research Centre at Washington University, which oversees a sizable collection of crosssectional and longitudinal brain MRI data from both demented and non-demented people, is the source of the OASIS dataset. Cross-sectional category comprises details of 416 patients between ages of 18 and 96, whereas the longitudinal dataset includes several scans of each subject across time. The mini-mental state examination (MMSE) and clinical dementia rating (CDR) are two tools that can be used to assess AD risk factors. With regard to risk factors, the participants are evaluated as having no dementia for CDR 0, very mild dementia for CDR

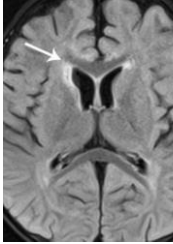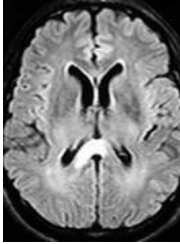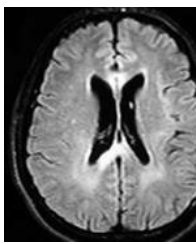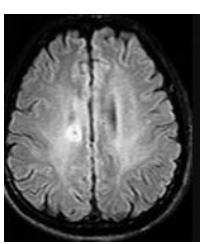0.5, mild dementia for CDR 1, and moderate dementia for CDT 2.

IBSR
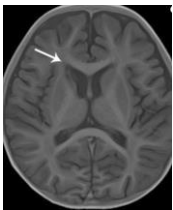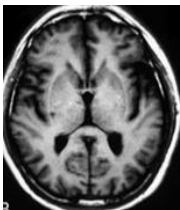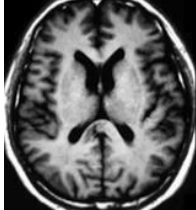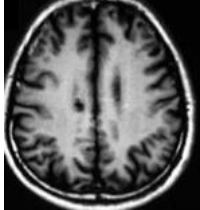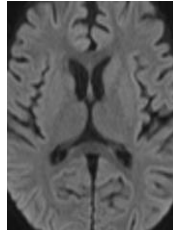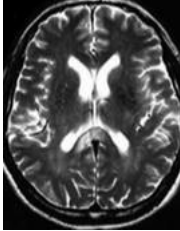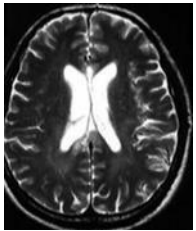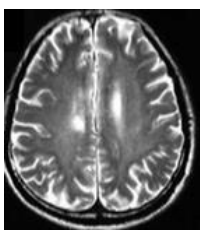
Brain image segmentation methods are tested and developed utilizing IBSR dataset. In addition to MRI data, this dataset offers findings from manually guided expert segmentation. Ground truth is made up of 20 actual T1-weighted (T1-W) MRIs with expert segmentation results that were manually guided. Approximately 60 coronal T1-W scans with a 3.1 mm resolution and 18 cortical T1-W slices with a 1.5 mm resolution are also included in each MRI volume. This dataset's subject volumes measure 256 × 256 × 128 pixels and have varying voxel spacings, measuring 0.84 × 0.84 × 1.5 mm3, 0.94 × 0.94 × 1.5 mm3, and 1.0 × 1.0 × 1.5 mm3. Additionally, 32 noncortical structures are manually segmented by Massachusetts General Hospital.

MICCAI

The 35 T1-w MRI volumes and the manual segmentation of 134 structures from

Neuromorphometrics, Inc., Scotts Valley, CA, USA, make up the MICCAI-2012 dataset. Tissue, tumour, and structural segmentation are its primary uses. In 2012, this dataset began with 80 fictitious and genuine cases. Over time, the training and testing data sets have grown in size. Sub-cortical structure segmentation is done utilizing MICCAI 2012 challenge in multi-atlas labelling.

9. Proposed model-based MRI brain image analysis

Table 2. Processing of input image utilizing proposed segmentation and classification methods

Input MRI image dataset	Input MRI image	Pre-processed image	Segmented image	Classified image
OASIS dataset				
IBSR dataset				
MICCAI dataset				

The processing of different input MRI image datasets for diagnosis of AD is displayed in Table 2 above. Here, classification output and processed image for a variety of datasets with chosen features are displayed. Figure 5 commonly uses a confusion matrix to determine these performance measures. This matrix represents both actual and anticipated categories. These performance metrics are frequently

calculated using a confusion matrix (see fig. 4). Actual and predicted classes are both covered by this matrix. Number of positive classifications that are correctly classified as positive is represented by True Positive (TP) values; number of negative classifications that are correctly classified as negative is represented by True Negative (TN) values; number of negative classifications that are incorrectly classified as positive is represented by False Positive (FP) values; number of positive classifications that are incorrectly classified as negative is represented by False Negative (FN) values.

Confusion matrix of OASIS dataset

Confusion matrix of IBSR   dataset

Confusion matrix of MICCAI
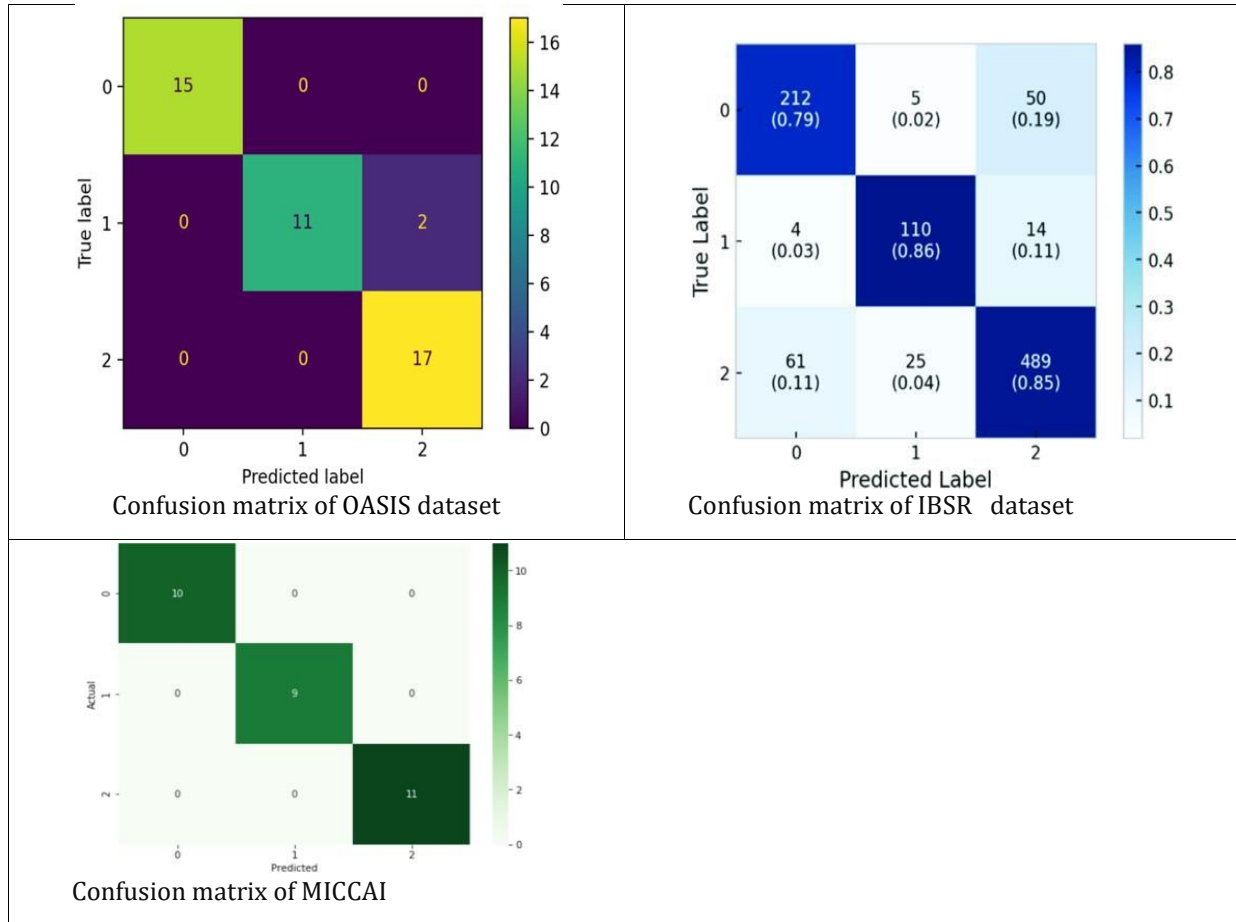
Figure 5: Confusion Matrix for Proposed MRI image dataset in Alzheimer's disease detection (a) OASIS (b) IBSR   dataset, (c) MICCAI

Comparative analysis based on MRI image in AD detection

Table 3. comparison for MRI image dataset in Alzheimer's disease detection

Dataset	Techniques	MMSE	Detection accuracy	WARR	Recall	AUC
OASIS	CNN	70	74	77	72	78
	RESNET	75	78	81	77	82
	PGWFO_FGCAHE-SVCGTVgg-16	81	85	85	84	86
IBSR Dataset	CNN	68	80	76	78	74
	RESNET	73	85	80	83	79
	PGWFO_FGCAHE-SVCGTVgg-16	82	90	86	87	85
MICCAI Dataset	CNN	78	84	84	79	75
	RESNET	83	87	89	88	83
	PGWFO_FGCAHE-SVCGTVgg-16	90	98	95	94	90

Table-2 shows analysis for MRI image dataset in AD detection. Here the MRI image dataset in AD detection analysed are OASIS, IBSR Dataset and MICCAI DATASET in terms of MMSE, Detection accuracy, WARR, Recall, AUC.
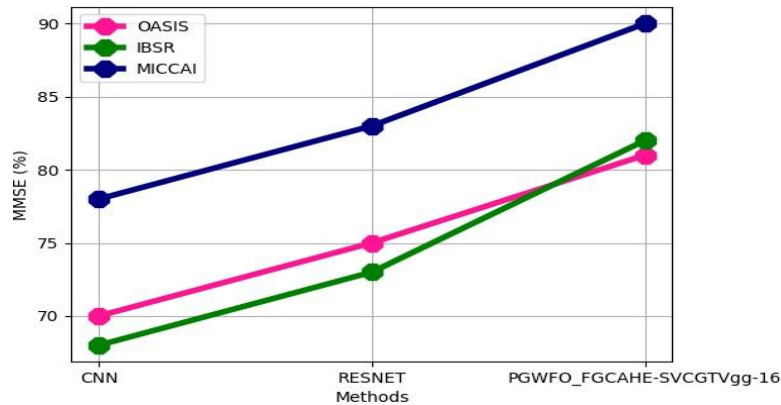

Figure 6. comparison of MMSE

The analysis for MMSE is displayed in Figure 6. Here, the proposed technique achieved 81% MMSE, 70% existing CNN, and 75% RESNET for OASIS dataset; for IBSR Dataset, proposed technique achieved 82% MMSE, 68% existing CNN, 73% RESNET; for MICCAI Dataset, proposed technique 90% MMSE, 78% existing CNN, and 83% RESNET.
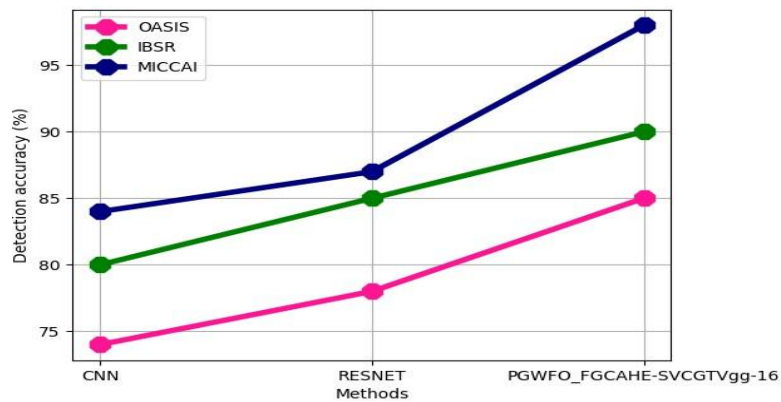

Figure 7. comparison of Detection accuracy

Figure 7 shows analysis in Detection accuracy. Here proposed technique Detection accuracy 85%, existing CNN 74%, RESNET 78% for OASIS dataset; for IBSR Dataset   proposed Detection accuracy 90%, existing CNN 80%, RESNET 85%; proposed technique Detection accuracy 98%, existing CNN 84%, RESNET 87% for MICCAI Dataset.
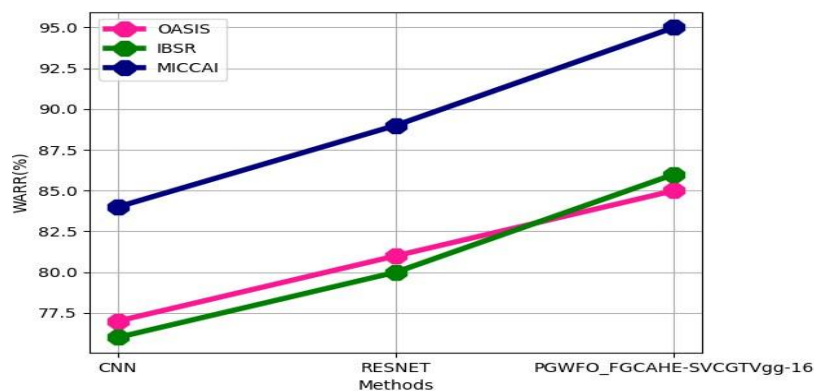

Figure 8. comparison of WARR

Analysis in WARR is shown in Figure 8. In the OASIS dataset, proposed technique WARR of 85%, existing CNN 77%, RESNET 81%; in IBSR   Plant dataset, proposed technique WARR 86%, existing CNN 76%, RESNET 80%; in MICCAI dataset, proposed technique WARR 95%, existing CNN 84%, RESNET 89%.
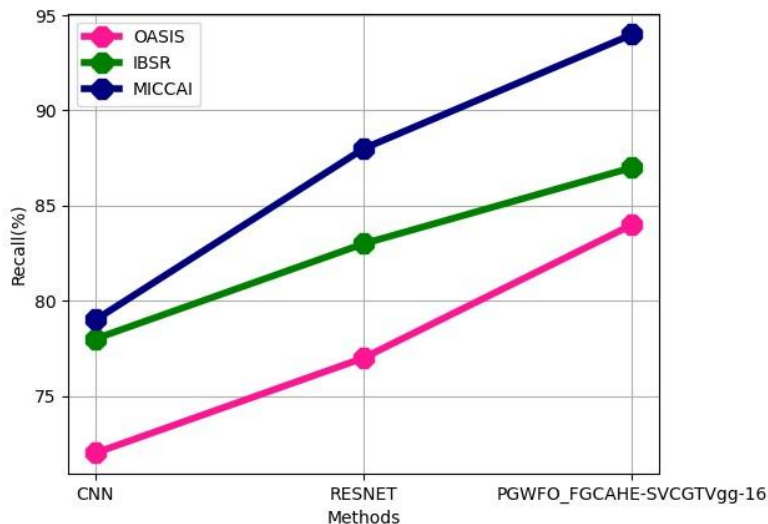

Figure 9. comparison of Recall

The recall analysis is displayed in Figure 9. Here, the proposed technique achieved 84% recall, 72% existing CNN, and 77% RESNET for OASIS dataset; for IBSR Dataset, proposed technique achieved 87% recall, 78% existing CNN, and 83% RESNET; for MICCAI Dataset, proposed technique 94% recall, 79% existing CNN, and 88% RESNET.
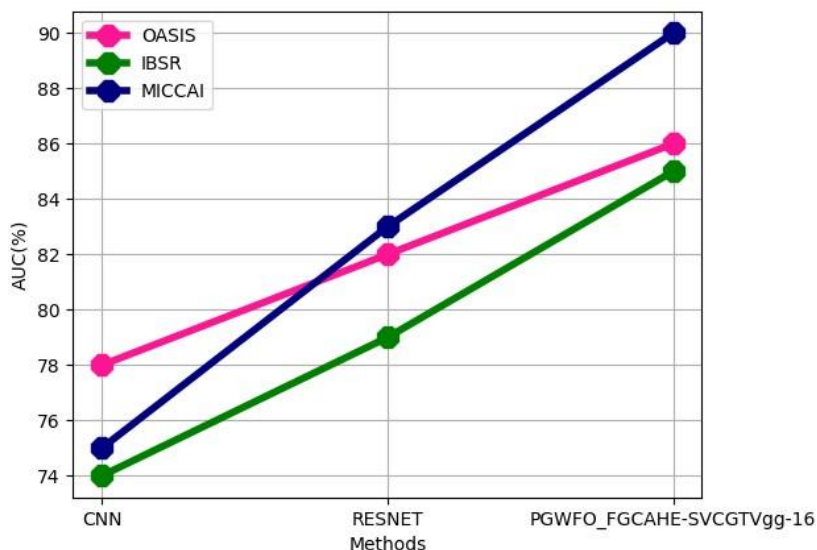

Figure 10. comparison of AUC

Figure 10 shows analysis in AUC. Here proposed technique AUC 86%, existing CNN 78%, RESNET 82% for OASIS dataset; for IBSR   Plant Dataset   proposed technique AUC 85%, existing CNN 74%, RESNET 79%; proposed technique AUC 90%, existing CNN 75%,
RESNET 83% for MICCAI Dataset. We were quite concerned about overfitting because of the size of the networks and the short amount of data that was used. To avoid overfitting of the network, the dropout technique is employed. Additionally, as the studies progressed, we saw that, around epoch 400, the error on training data continued to decrease, while the validation loss began to rise to a significant value. Early pausing is therefore used in training to prevent overfitting.

DISCUSSION
In this case, accuracy is defined as the percentage of subjects categorized properly throughout the entire population. The percentage of Alzheimer's class participants who were correctly diagnosed out of all the

participants is known as sensitivity, also known as recall. The percentage of non-Alzheimer's class subjects properly classified out of all non-Alzheimer's class subjects is known as specificity. Models in this study aim to achieve the ideal value of 1, which is represented by these measures. TP is when the model accurately predicts the

Alzheimer's subject class. When a model mistakenly assumes that an instance of a non-

Alzheimer's class is an instance of Alzheimer's class, it produces a FP, also known as a TypeI error. FN, also known as Type-II errors, occur when a method predicts an instance of Alzheimer's class mistakenly as a non-Alzheimer's class instance. Last but not least, TN happens when method accurately predicts an instance of a class other than Alzheimer's. Generally speaking, we compute these metrics using the models that have best validation set accuracies.

CONCLUSION

To optimize the identification of AD, this research aims to present a unique technique for MRI brain picture segmentation and classification utilising a metaheuristic model and deep learning technique. The dataset was gathered and subjected to fuzzy Gaussian C-adaptive histogram equalization for noise removal and dataset segmentation in the suggested model. Subsequently, the picture segmentation process was carried out utilising support vector convolutional graph transfer VGG-16 learning for classification, and particle grey wolf firefly optimisation for optimisation. We discovered that transfer learning methods performed better on this task. After looking into class imbalance as well as data leakage issues more, we discovered that they have a tendency to make the classification performance bias worse. The experimental findings demonstrate that, in comparison to earlier studies using classical horizontal plane MRI, the model performs satisfactorily, particularly when it comes to identifying the early stages of AD. Because of low phenotypic manifestation, more significantly, early stages of therapy's improved efficacy, these are the hardest stages to detect. People should be made aware of this illness and encouraged to have themselves checked up. Our current project is to implement this approach on a website for more useful applications. This model can be evaluated on a bigger dataset in the future. For training and testing, available dataset for 'Moderate Demented' class contained just 52 and 12 photos, respectively.

REFERENCE

[1]   Arafa, D. A., Moustafa, H. E. D., Ali, H. A., Ali-Eldin, A. M., &Saraya, S. F. (2024). A deep learning framework for early diagnosis of Alzheimer's disease on MRI images. Multimedia Tools and Applications, 83(2), 3767-3799.

[2]   Lahmiri, S. (2023). Integrating convolutional neural networks, kNN, and Bayesian optimization for efficient diagnosis of Alzheimer's disease in magnetic resonance images. Biomedical Signal Processing and Control, 80, 104375.

[3]   Jamalullah, R. S., Gladence, L. M., Ahmed, M. A., Lydia, E. L., Ishak, M. K., Hadjouni, M., & Mostafa, S. M. (2023). Leveraging brain mri for biomedical alzheimer's disease diagnosis using enhanced manta ray foraging optimization based deep learning. IEEE Access.

[4]   Pradhan, N., Sagar, S., & Singh, A. S. (2024). Analysis of MRI image data for Alzheimer disease detection using deep learning techniques. Multimedia Tools and Applications, 83(6), 17729-17752.

[5]   Borkar, P., Wankhede, V. A., Mane, D. T., Limkar, S., Ramesh, J. V. N., & Ajani, S. N. (2023). Deep learning and image processing-based early detection of Alzheimer disease in cognitively normal individuals. Soft Computing, 1-23.

[6]   Marwa, E. G., Moustafa, H. E. D., Khalifa, F., Khater, H., &AbdElhalim, E. (2023). An MRI-based deep learning approach for accurate detection of Alzheimer's disease. Alexandria Engineering Journal, 63, 211-221.

[7]   Yao, Z., Wang, H., Yan, W., Wang, Z., Zhang, W., Wang, Z., & Zhang, G. (2023). Artificial intelligence-based diagnosis of Alzheimer's disease with brain MRI images. European Journal of Radiology, 165, 110934.

[8]   Shamrat, F. J. M., Akter, S., Azam, S., Karim, A., Ghosh, P., Tasnim, Z., ... & Ahmed, K. (2023). AlzheimerNet: An effective deep learning based proposition for alzheimer's disease stages classification from functional brain changes in magnetic resonance images. IEEE Access, 11, 16376-16395.

[9]   Rana, M. M., Islam, M. M., Talukder, M. A., Uddin, M. A., Aryal, S., Alotaibi, N., ... & Moni, M. A. (2023). A robust and clinically applicable deep learning model for early detection of Alzheimer's. IET Image Processing, 17(14), 3959-3975.

[10] Chinnasamy, P., Sathya, K. B., Jebamani, B. J., Nithyasri, A., &Fowjiya, S. (2023). Deep Learning: Algorithms, Techniques, and Applications — A Systematic Survey. In L. Ashok Kumar, D. KarthikaRenuka, & S. Geetha (Eds.), Deep Learning Research Applications for Natural Language Processing (pp. 1-17). IGI Global. https://doi.org/10.4018/978-1-6684-6001-6.ch001.

[11] E. Anupriya, M. Thaile, P. Chinnasamy and M. L. Narayana, "Heart Diseases Prediction Using Machine Learning Algorithms," 2023 International Conference on Computer Communication and Informatics (ICCCI), Coimbatore, India, 2023, pp. 15, doi: 10.1109/ICCCI56745.2023.10128590.

[12] Chinnasamy, P., Wong, W. K., Raja, A. A., Khalaf, O. I., Kiran, A., &Babu, J. C. (2023). Health recommendation system using deep learning-based collaborative filtering. Heliyon, 9(12).

[13] Yao, Z., Mao, W., Yuan, Y., Shi, Z., Zhu, G., Zhang, W., ... & Zhang, G. (2023). Fuzzy-VGG: A fast deep learning method for predicting the staging of Alzheimer's disease based on brain MRI. Information Sciences, 642, 119129.

[14] Arya, A. D., Verma, S. S., Chakarabarti, P., Chakrabarti, T., Elngar, A. A., Kamali, A. M., &Nami, M. (2023). A systematic review on machine learning and deep learning techniques in the effective diagnosis of Alzheimer's disease. Brain Informatics, 10(1), 17.

[15] Sorour, S. E., Abd El-Mageed, A. A., Albarrak, K. M., Alnaim, A. K., Wafa, A. A., &

[16] El-Shafeiy, E. (2024). Classification of Alzheimer's disease using MRI data based on Deep Learning Techniques. Journal of King Saud University-Computer and Information Sciences, 36(2), 101940.

[17] Illakiya, T., &Karthik, R. (2023). Automatic detection of Alzheimer's disease using deep learning models and neuro-imaging: current trends and future perspectives. Neuroinformatics, 21(2), 339-364.

[18] Kaya, M., &Çetin-Kaya, Y. (2024). A Novel Deep Learning Architecture Optimization for Multiclass Classification of Alzheimer's Disease Level. IEEE Access.

[19] Singh, A., & Kumar, R. (2024). Brain MRI Image Analysis for Alzheimer's Disease (AD) Prediction Using Deep Learning Approaches. SN Computer Science, 5(1), 160.

[20] Saeedi, S., Rezayi, S., Keshavarz, H., & R. NiakanKalhori, S. (2023). MRI-based brain tumor detection using convolutional deep learning methods and chosen machine learning techniques. BMC Medical Informatics and Decision Making, 23(1), 16.

[21] Roopa, Y. M., Reddy, B. B., Babu, M. R., &Nayak, R. K. (2023). Teaching learningbased brain storm optimization tuned Deep-CNN for Alzheimer's disease classification. Multimedia Tools and Applications, 82(21), 33333-33356.

[22] Sampath, R., &Baskar, M. (2024). Alzheimer's Disease Prediction Using FlyOptimized Densely Connected Convolution Neural Networks Based on MRI Images. The Journal of Prevention of Alzheimer's Disease, 1-16.

[23] Bamber, S. S., &Vishvakarma, T. (2023). Medical image classification for Alzheimer's using a deep learning approach. Journal of Engineering and Applied Science, 70(1), 54.

[24] Rallabandi, V. S., &Seetharaman, K. (2023). Deep learning-based classification of healthy aging controls, mild cognitive impairment and Alzheimer's disease using fusion of MRI-PET imaging. Biomedical Signal Processing and Control, 80, 104312.

[25] Odusami, M., Maskeliūnas, R., Damaševičius, R., &Misra, S. (2023). Explainable deep-learning-based diagnosis of Alzheimer's disease using multimodal input fusion of PET and MRI Images. Journal of Medical and Biological Engineering, 43(3), 291302.

[26] Gupta, M., Kumar, R., & Abraham, A. (2024). Adversarial Network-Based Classification for Alzheimer's Disease Using Multimodal Brain Images: A Critical Analysis. IEEE Access.

[27] Shojaei, S., Abadeh, M. S., &Momeni, Z. (2023). An evolutionary explainable deep learning approach for Alzheimer's MRI classification. Expert systems with applications, 220, 119709.

[28] Matlani, P. (2024). BiLSTM-ANN: early diagnosis of Alzheimer's disease using hybrid deep learning algorithms. Multimedia Tools and Applications, 83(21), 6076160788.

[29] Leela, M., Helenprabha, K., &Sharmila, L. (2023). Prediction and classification of Alzheimer disease categories using integrated deep transfer learning approach. Measurement: Sensors, 27, 100749.

[30] P. Chinnasamy, S. Arun Kumar, V. Navya, K. Lakshmi Priya, Siva SruthiBoddu, Machine learning based cardiovascular disease prediction, Materials Today: Proceedings, Volume 64, Part 1, 2022, Pages 459-463, ISSN 22147853,https://doi.org/10.1016/j.matpr.2022.04.907.